Activation of Methane on PdZn/C Electrocatalysts in an Acidic Electrolyte at Low Temperatures

J. Nandenha[1,*], I.H.F. Nagahama[1,2], J.Y. Yamashita[1,2], E.H. Fontes[1], J.M.S. Ayoub[1], R.F.B. de Souza[1], F.C. Fonseca[1], A.O. Neto[1,*]

[1] Instituto de Pesquisas Energéticas e Nucleares, IPEN/CNEN-SP, Av. Prof. Lineu Prestes, 2242 Cidade Universitária, CEP 05508-000, São Paulo, SP, Brazil
[2] Faculdades Osvaldo Cruz, FOC, Rua Brigadeiro Galvão, 540 Barra Funda, CEP 01151-000, São Paulo, SP, Brazil
*E-mail: neto.almir@bol.com.br

PdZn/C electrocatalysts were prepared by sodium borohydride utilized as reducing agent for activation methane in an acidic medium at room temperature and in a proton exchange membrane fuel cell (PEMFC) at 80°C. The materials prepared were characterized by X-ray diffraction (XRD), transmission electron microscopy (TEM) and X-ray photoelectron spectroscopy (XPS). The diffractograms of the PdZn/C electrocatalysts showed only peaks associated with Pd face-centered cubic (fcc) structure. Cyclic voltammograms (CV) of all electrocatalysts after adsorption of methane shown an increment in current during the anodic scan, this effect was more pronounced for $Pd_{(70)}Zn_{(30)}$/C. In situ ATR-FTIR (Attenuated Total Reflectance-Fourier Transform Infrared) experiments was not observed the formation of intermediates adsorbed for PdZn/C electrocatalysts, this behavior indicated that the methane oxidation occurs by parallel mechanisms. Polarization curves at 80°C in PEMFC show that $Pd_{(90)}Zn_{(10)}$/C has superior performance over the other electrocatalysts in methane oxidation.

1. INTRODUCTION

Methane is a constituent of natural gas. It has higher energy per mass unit (55.7 kJ g^{-1}) compared to other hydrocarbons or combustible. Consequently, the use of methane as combustible in SOFC fuel cell has attracted attention [1]. The advances in drilling technologies have expanded access to natural gas and reduced the expense of process [1, 2]. The use of methane in the energy sector has

been via combustion. However, a new alternative is to use methane in a Proton Exchange Membrane Fuel Cells (PEMFCs).

The Fuel cells are more efficient than heat engines at the lower temperature, and their exhaust is composed of only CO_2 and water making them attractive, and clean energy conversion devices [1]. In the fuel cell technology, methane it is used after steam reforming or directly in Solid Oxide Fuel Cell (SOFC) [3]. Nevertheless, the high operating temperature (600 - 1,100^{o}C) of a SOFC leads to problems, like carbon deposition, and requires high startup time. Therefore, the use of methane directly in a PEMFC could be more attractive [4].

Proton Exchange Membrane Fuel Cells (PEMFCs) has the advantage to much higher power densities, operating flexibility (faster start up and shut down), and has the potential to be used in different scales, i.e., from micro to large-scale distributed power generation. This operation makes the activation of methane extremely challenging under the operating conditions of the PEMFC, where the development of new nanomaterials is fundamental [1, 4].

The inherent chemical properties of methane, including low electron and proton affinity, low polarizability, weak acidity, high C-H bond energy (439 kJ mol^{-1}) as well as high ionization energy [5, 6], make it very inert. One of the biggest challenges concerning the use of methane in a PEMFCs is the development of catalysts that provide sufficient rates of C-H activation at operating temperatures in the range of 60 to 100°C [1, 7-9].

The activation of C-H and C-C bonds in hydrocarbons by various transition-metal oxide ions has been investigated experimentally and theoretically by several authors [4, 10-13]. The electrochemical oxidation of methane at low-temperature fuel cell is a slow process that has been received little attention by the scientific community in recent years [14, 15].

Joglekar et al. [1] showed that the development of a platinum organometallic complexes covalently anchored to ordered mesoporous carbon (OMC) for electrochemical oxidation of methane in a PEMFC at 80°C, in which was obtained a power density of 403 µW/mg. Pt organometallic was five times higher than the power density observed from a modern commercial catalyst and two orders of magnitude higher than that from a Pt black catalyst.

Platinum (Pt) and Pt-based electrocatalysts are the essential materials for both anode and cathode fuel cells in acidic media. However, some challenges associated with Pt, such as high-cost and scarcity of Pt, poisoning by CO, and slow kinetics limit their use [4, 16-18]. An alternative to Pt is the use of Pd, which it is relatively more abundant in the earth's crust [16, 19]. Pd and Pd alloys exhibit lower CO poisoning in alkaline media; therefore their use would reduce the cost of the electrode materials [16, 20-22]. Nevertheless, the direct electrochemical oxidation of methane at ambient temperatures has been experimentally demonstrated by some works with palladium [14, 23]. The Pd or other metals of Pd group metals are frequently employed as anodic electrodes for the activation of methane operating with polymer electrolyte membranes [14, 24], alkaline [25, 26] or acid electrolytes [23].

Nandenha et al. [4] synthesized Pt/C, Pt/C-ATO, Pd/C and Pd/C-ATO electrocatalysts for methane oxidation in an acidic electrolyte at 25°C and in a direct methane proton exchange membrane fuel cell at 80°C. They observed the presence of oxygenated species, like CO or -CHO, which indicates the formation of carbon dioxide species coming from methane oxidation. They have

concluded that Pd/C and Pt/C showed superior performance for methane oxidation in Direct Methane Fuel Cell (DMEFC), while Pd/C-ATO and Pt/C-ATO indicated a decrease in kinetics reaction showing that why Pd/C has a better open circuit voltage when was compared to the other materials above-mentioned.

Matin et al. [16] prepared PdZn/C for methanol oxidation reaction in an alkaline medium and observed that PdZn/C showed an improved electrocatalytic activity by a factor of ~1.4 - 1.9 in comparison with Pd/C synthesized using the same method. The methanol oxidation reaction in PdZn/C started at an earlier onset potential and has a higher current density than for Pd/C [16].

Zhang et al. [27] prepared a Pd-Zn nanocrystals with particle diameters of approximately 5.0 - 6.5 nm. The electrochemical measurements showed that the Pd_xZn_{1-x} nanocrystals exhibit superior performance (activity and stability) for the formic acid oxidation reaction compared with commercial Pd/C. These authors concluded that the better performance of Pd_xZn_{1-x} could be attributed to the synergistic effect between Pd and Zn in Pd-Zn nanocrystals.

Li et al. [28] synthesized palladium nanoparticles (PdNPs) using n-alkylamines (C_n-NH_2) as a stabilizing ligand. These authors showed that the PdNPs were more activity and stable to CH_4 when compared to the bare Pd electrodes.

The aim of our work was to synthesize Pd/C, Zn/C, $Pd_{(90)}Zn_{(10)}$/C, $Pd_{(70)}Zn_{(30)}$/C and $Pd_{(50)}Zn_{(50)}$/C electrocatalysts by sodium borohydride reduction process for activation of methane in acidic electrolytes, where the electrochemical activity and the mechanism were studied in the temperature room, and, finally the electrocatalysts were also applied in the Proton Exchange Membrane Fuel Cells (PEMFC).

2. EXPERIMENTAL METHODS

2.1. Chemicals

The reagents palladium(II) nitrate hydrate ($Pd(NO_3)_2.2H_2O$, 97%) and zinc nitrate hydrate ($Zn(NO_3)_2.xH_2O$, 99.999%) were purchased from Sigma-Aldrich, and 2-propanol (C_3H_7OH, 99.5%) was purchased from Alphatec. Sodium borohydride ($NaBH_4$, ≥ 98,0%), Sodium hydroxide (NaOH, 98%) and Vulcan XC72 carbon black (BET surface area = 250 m^2 g^{-1}) were purchased from Aldrich, Alphatec and Cabot Corporation, respectively. All the reagents were used without any further purification. Ultrapure water (Millipore, 18.2 MΩ cm) was used for the entire study.

2.2. Synthesis

Pd/C, Zn/C, $Pd_{(90)}Zn_{(10)}$/C, $Pd_{(70)}Zn_{(30)}$/C and $Pd_{(50)}Zn_{(50)}$/C electrocatalysts with 20% of metal loading, were prepared using $Pd(NO_3)_2.2H_2O$ (Fluka) and $Zn(NO_3)_2·xH_2O$ (Sigma-Aldrich) as metal sources and sodium borohydride ($NaBH_4$, Aldrich) as reducing agent and Vulcan Carbon XC72 (Cabot) was used as support [29]. The Vulcan XC72 was dispersed into a solution of water/2-propanol (50/50, v/v), containing metal ions of Pd or Zn. The solution resulting was submitted to an ultrasonic

bath by 10 minutes, and then the NaBH$_4$ solution in 0.01 mol L^{-1} NaOH was added. The resulting solution was then maintained under stirring for an additional 1 hour. Finally, the material was filtered, and washed with ultrapure water and dried at 70°C for 2 hours [4, 30].

2.3. X-ray Diffraction (XRD) and Transmission Electron Microscopy (TEM)

Pd/C, Zn/C, Pd$_{(90)}$Zn$_{(10)}$/C, Pd$_{(70)}$Zn$_{(30)}$/C and Pd$_{(50)}$Zn$_{(50)}$/C electrocatalysts were characterized by X-ray diffraction analysis using CuKα radiation source (λ = 0.15406 nm). The diffractograms were recorded in the range of 2θ = 20$°$ to 90$°$ with a step size of 0.05$°$ and a scan time of 2 seconds per step [4, 31, 32]. The morphology and nanoparticle distribution of electrocatalysts were determined by transmission electron microscopy using a JEOL electron microscope model JEM-2100 operated at 200 kV. After, the mean nanoparticle sizes were measured over 300 nanoparticles from 10 micrographs.

2.4. X-ray Photoelectron Spectroscopy (XPS)

X-ray Photoelectron Spectroscopy was performed using the X-ray Photoelectron Spectrometer K-Alpha (Thermo Scientific) at LNNANO (Laboratório Nacional de Nanotecnologia) facility held in Campinas/SP and maintained by CNPEM (Centro Nacional de Pesquisa em Energia e Materiais). The X-ray spot size was set to 400 μm. The powder samples were held in a copper ribbon. The final core XPS spectra were an average of three random areas at the surface of the electrocatalysts. To characterize the metals and its oxidation states we used the most intense band corresponding to a singlet or doublet states.

2.5. Cyclic Voltammetry (CV)

The cyclic voltammetry of electrocatalysts were carried out with an AutoLab PGSTAT30 Potentiostat/Galvanostat, at 25ºC in a 0.5 mol L^{-1} H$_2$SO$_4$ solution using a three-electrodes conventional cell. The reversible hydrogen electrode (RHE) was used as a reference electrode, a Pt wire as a counter electrode and a thin porous coating technique as working electrode as previously reported [4]. The cyclic voltammetry experiments were done at a scan rate of 10 mV s^{-1} for the potential range of 0.05 to 1.2 V with the presence or absence of methane. The adsorption of methane was realized at 0.05 V with bubbling for 1,800 seconds in 0.5 mol L^{-1} H$_2$SO$_4$ [4].

2.6. Atennuated Total Reflection - Fourier Transform Infrared (ATR-FTIR)

The ATR-FTIR measurements were performed on a spectrometer equipped with an MCT detector cooled with liquid N$_2$. The ATR accessory with internal reflection element Diamond/ZnSe is coupled to the spectrometer [33], where an electrochemical cell is connected above the internal reflection element. The working electrode was an ultrathin porous coating technique in the presence of

CH$_4$ gas saturated in 0.5 mol L^{-1} H$_2$SO$_4$ for 1,800 seconds. The background spectra were collected following Nandenha works [4].

2.7. Fuel Cell Experiment

The methane studies in the PEMFC were made in a single cell with an area of 5 cm^2. The temperatures were set to 80ºC for the fuel cell and 85ºC for the methane humidifier and 85ºC for the oxygen humidifier. The fuel was 500 mL of 99% methane gas at approximately 150 mL min^{-1}, the oxygen flow was regulated at 200 mL min^{-1} and pressure atmospheric was also set. Polarization curves were obtained using an AutoLab PGSTAT302N Potentiostat/Galvanostat with Software NOVA 2.1.2 coupled, and connected in the fuel cell. Membrane Electrode Assemblies (MEAs) were prepared by hot pressing at 125°C for 5 min under pressure of 225 kgf cm^{-2} using a pretreated Nafion® 117 membranes placed between anode (Pd/C, Zn/C, Pd$_{(90)}$Zn$_{(10)}$/C, Pd$_{(70)}$Zn$_{(30)}$/C and Pd$_{(50)}$Zn$_{(50)}$/C) and cathode with Pt/C BASF electrocatalysts. The binary anode electrodes and the cathode prepared in this work were made with 1 mg Pd cm^{-2} or 1 mg Pt cm^{-2} electrocatalyst loading, respectively [29, 32].

3. RESULTS AND DISCUSSION

Figure 1 shows the X-ray diffractograms of the Pd/C, Zn/C, Pd$_{(90)}$Zn$_{(10)}$/C, Pd$_{(70)}$Zn$_{(30)}$/C and Pd$_{(50)}$Zn$_{(50)}$/C electrocatalysts. For all electrocatalysts prepared are observed a broad peak at about 2θ ≈ 25° that are associated with the Vulcan Carbon XC72 support material. For Pd/C and PdZn/C electrocatalysts were observed four peaks at about 2θ ≈ 40°, 47°, 67° and 82°, which are associated with the (111), (200), (220) and (311) crystal planes, respectively, characteristic of the face-centered cubic structure (fcc) of palladium (Pd) JCPDS #46-1043 [4, 34]. The presence of other seven peaks in the Zn/C patterns at 2θ values of 32º, 34º, 36º, 48º, 57º, 63º and 68º were attributed to the (100), (002), (101), (102), (110), (103) and (112) planes, respectively, which are characteristic of the hexagonal structure of ZnO JCPDS #36-1451 [16, 35].

For Zn/C electrocatalyst no peaks related to Zn were observed, therefore the presence of Zn in small amounts and amorphous forms cannot be discarded; however, XPS results may indicate its presence. All PdZn/C electrocatalysts showed a shift to higher angles of the peak associated to the (200), (220) and (311) planes compared to those of Pd/C (see Fig. 1). This indicates that after incorporation of Zn into the Pd lattice to form the Pd-Zn alloys, there were significant shifts in the diffraction peak positions due to the smaller ion radius of Zn, following the results of Zhang et al. and Conant et al. works [27, 36].
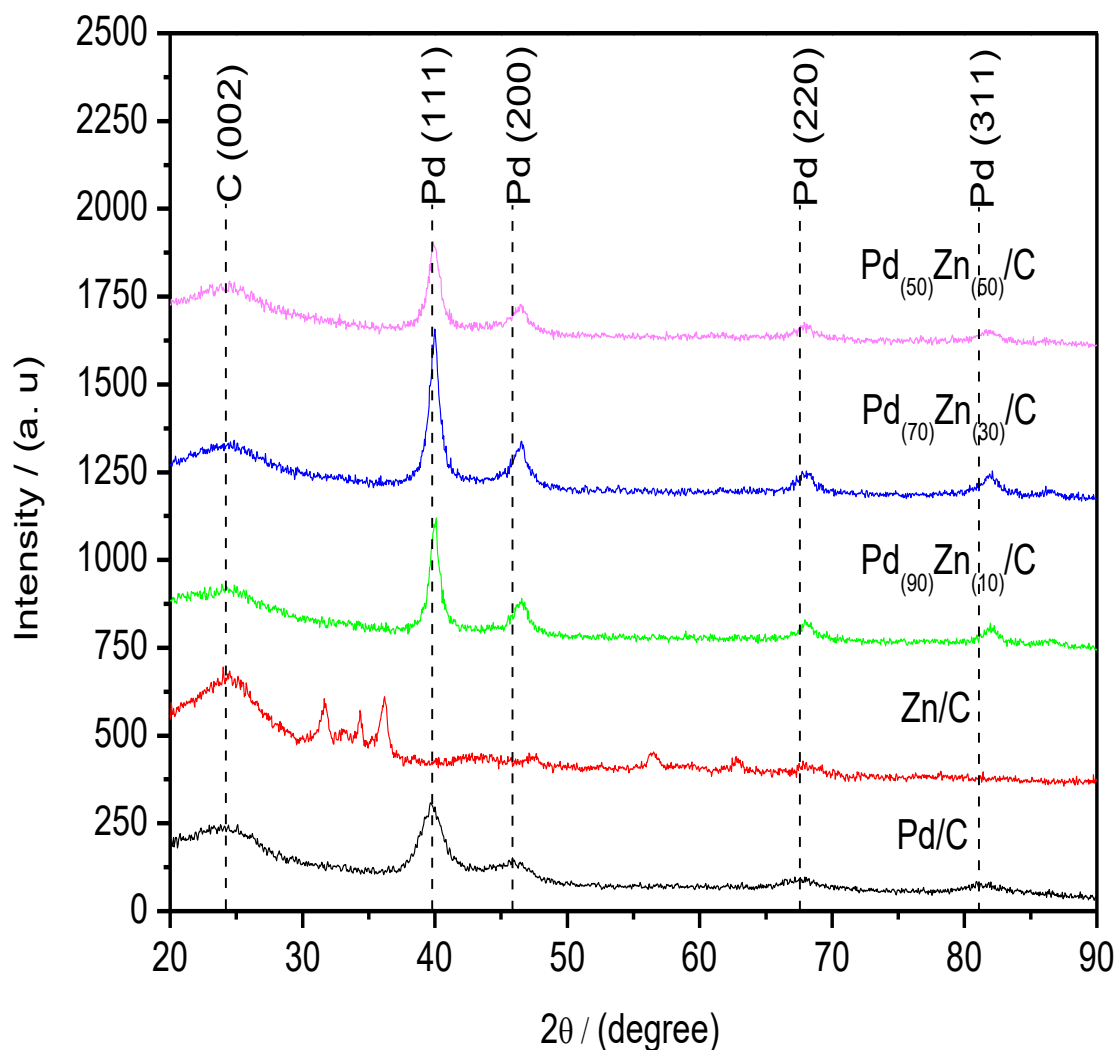
Figure 1. X-ray diffractograms of the Pd/C, Zn/C, Pd$_{(90)}$Zn$_{(10)}$/C, Pd$_{(70)}$Zn$_{(30)}$/C and Pd$_{(50)}$Zn$_{(50)}$/C electrocatalysts prepared by borohydride reduction process.
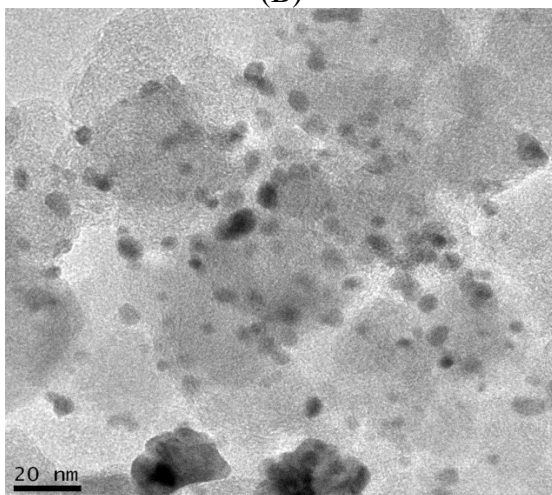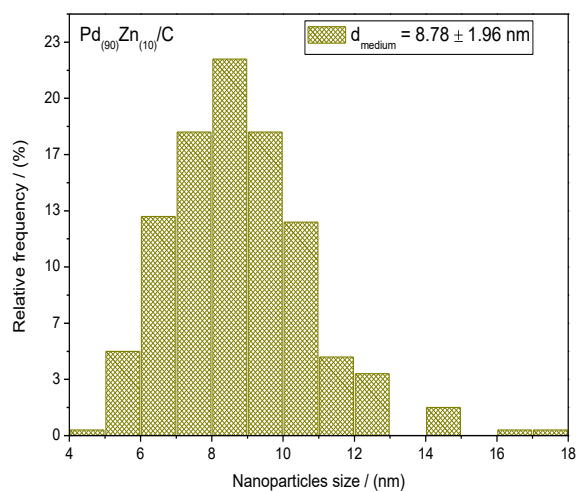
TEM micrographs and histograms of the nanoparticle diameters distribution of Pd/C and PdZn/C electrocatalysts are shown in Figure 2. All images showed that the nanoparticles where well dispersed on the support, but some agglomerates were present. The mean nanoparticle diameters of Pd/C, Pd$_{(90)}$Zn$_{(10)}$/C, Pd$_{(70)}$Zn$_{(30)}$/C and Pd$_{(50)}$Zn$_{(50)}$/C electrocatalysts were 7.92, 8.78, 8.79, and 8.78 nm, respectively (Fig. 2). The insertion of Zn content in Pd/C electrocatalysts increased mean nanoparticle diameter. This increase is due to the electrocatalyst sintering, and also due to the presence of the second metal Zn in the whole nanoparticle incorporated into the lattice structure, confirmed by XRD. This behavior has also been observed by Conant et al. and Nandenha et al. [36, 37].
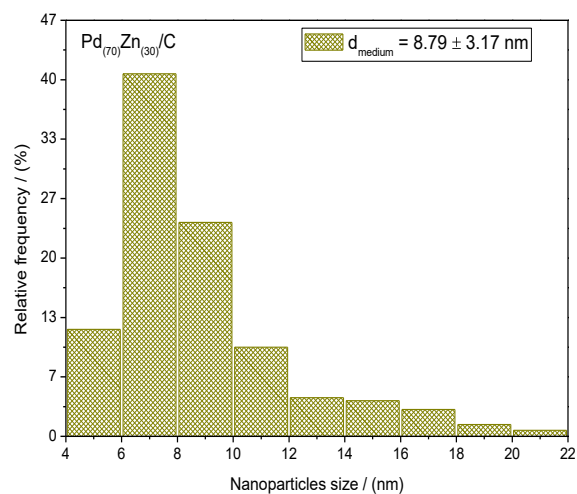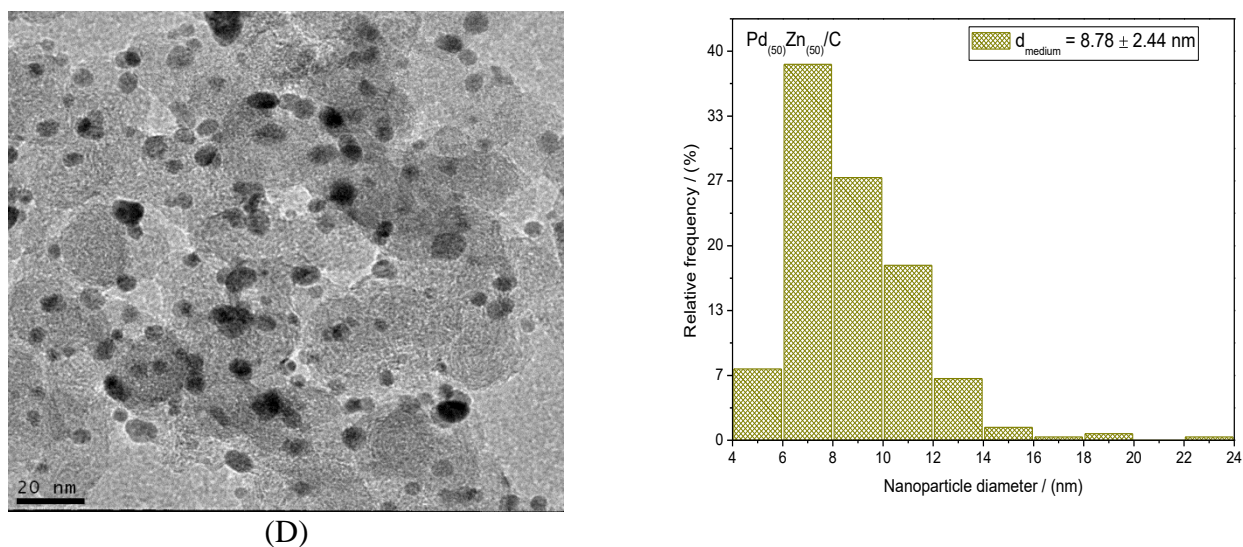
(D)
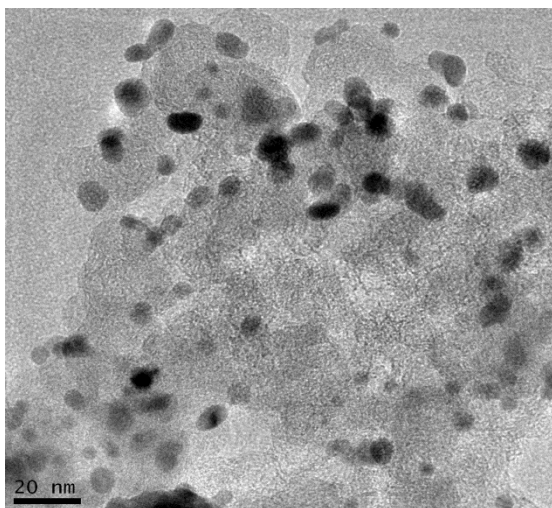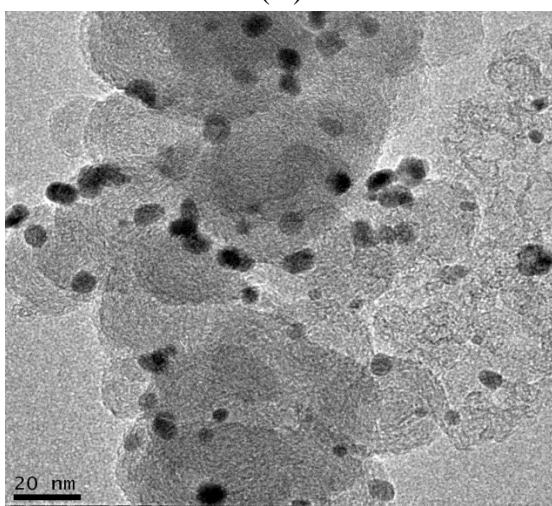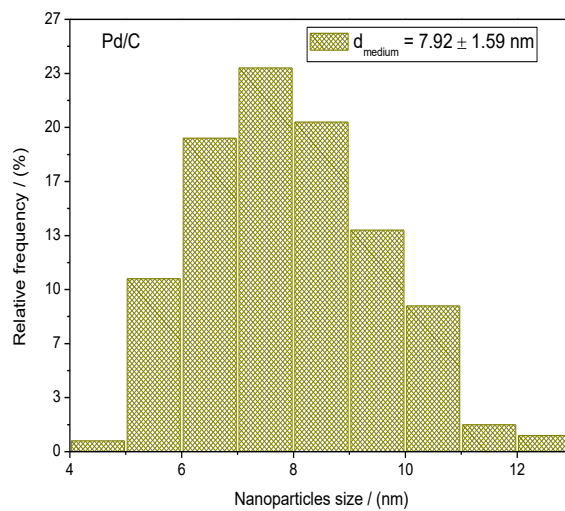
Figure 2. TEM micrographs and a histograms of **(A).** Pd/C, **(B).** $Pd_{(90)}Zn_{(10)}$/C, **(C).** $Pd_{(70)}Zn_{(30)}$/C and **(D).** $Pd_{(50)}Zn_{(50)}$/C electrocatalysts.

Figure 3 show the core level XPS spectra of Pd3d and Zn2p for Pd/C, Zn/C, $Pd_{(90)}Zn_{(10)}$/C, $Pd_{(70)}Zn_{(30)}$/C and $Pd_{(50)}Zn_{(50)}$/C. For all of them, according to the Pd3d core level spectra, was possible to observe the presence of Pd^0 and PdO, which can be ascribed to the long-time exposure to the oxygen during the metal salts reduction (PdO formation) [38], and to the use of a strong reducing agent (Pd^0 formation) [39]. The atomic concentration of Zn in $Pd_{(90)}Zn_{(10)}$/C is too low, so it was not possible to distinguish the different oxidation states.

Zn/C and $Pd_{(50)}Zn_{(50)}$/C showed the presence of ZnO, but $Pd_{(70)}Zn_{(30)}$/C and $Pd_{(90)}Zn_{(10)}$/C don't. The SNR of Zn2p for these materials is too low compared to the other ones, mainly because of the lower atomic concentration of Zn, i.e., 30% and 10%. $Pd_{(70)}Zn_{(30)}$/C and $Pd_{(90)}Zn_{(10)}$/C has the lowest amount of Zn, so the probability for them to have more available Pd active sites is higher, which can explain, qualitatively, why $Pd_{(70)}Zn_{(30)}$/C has a better performance in electrochemical experiments. For instance, shows that the support can decrease the surface area of the Pd atoms [40], confirming our argument that as higher the atomic concentration of the co-catalyst, the lower active surface of the electrocatalyst, causing a decrease in the electrochemical activity. Figure 4 shows a comparison of cyclic voltammetry results of Pd/C, Zn/C, $Pd_{(90)}Zn_{(10)}$/C, $Pd_{(70)}Zn_{(30)}$/C and $Pd_{(50)}Zn_{(50)}$/C electrocatalysts immersed in 0.5 mol L^{-1} H_2SO_4 electrolyte at the scan rate of 10 mV s^{-1}. The sharp peaks observed for Pd/C, $Pd_{(90)}Zn_{(10)}$/C, $Pd_{(70)}Zn_{(30)}$/C and $Pd_{(50)}Zn_{(50)}$/C electrocatalysts showed a well-defined hydrogen adsorption/desorption region which are attributed to the oxidation of the adsorbed hydrogen on the Pd surface (peaks in the range of 0.05 to 0.4 V vs RHE). The voltammograms of Zn/C is suppressed in comparison with others electrocatalysts prepared indicating the characteristics of Zn. However, these results suggest that Zn help to stabilize the PdO phase resulting in better thermal stability of the most active PdO phase [41].
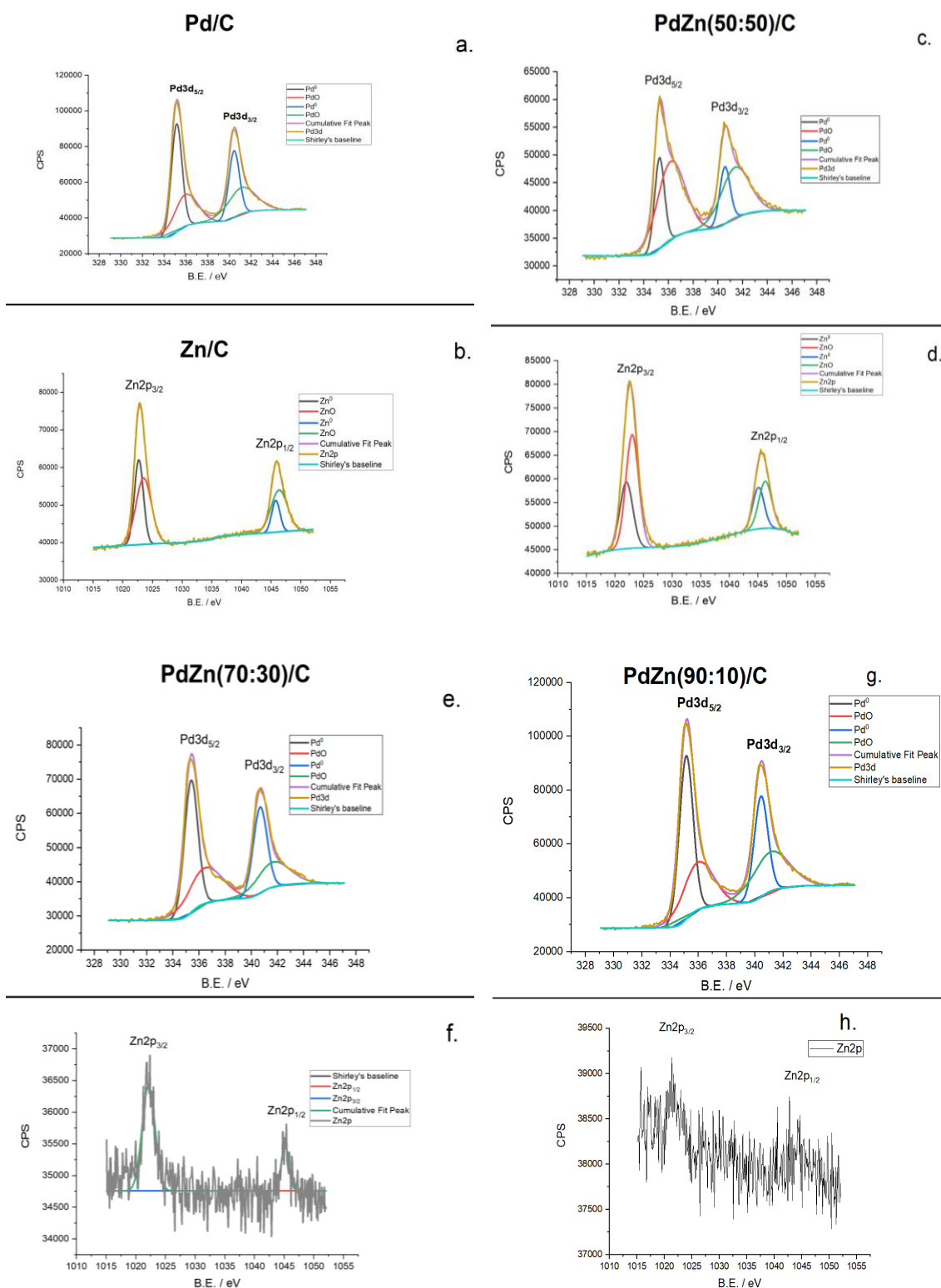
Figure 3. XPS spectra of (**a**). Pd3d spectra of Pd/C and its oxidation states. (**b**). Zn2p spectra of Zn/C and its oxidation states. (**c**). Pd3d spectra of $Pd_{(50)}Zn_{(50)}$/C and its oxidation states, (**d**). Zn2p spectra of $Pd_{(50)}Zn_{(50)}$/C and its oxidation states. (**e**). Pd3d spectra of $Pd_{(70)}Zn_{(30)}$/C and its oxidation states, (**f**). Zn2p spectra of $Pd_{(70)}Zn_{(30)}$/C. (**g**). Pd3d spectra of $Pd_{(90)}Zn_{(10)}$/C and its oxidation states, (**h**). Zn2p spectra of $Pd_{(90)}Zn_{(10)}$/C.

For $Pd_{(70)}Zn_{(30)}/C$, was observed an increase in the current values in the double layer (0.30 - 0.85 V) in comparison with Pd/C, $Pd_{(90)}Zn_{(10)}/C$ and $Pd_{(50)}Zn_{(50)}/C$, indicating more formation of Pd and Zn oxide species. For Pd/C and all PdZn/C eletrocatalysts, the negative scan also showed an increase in currents at the double layer at about 0.7 V. This could be associated with the reduction of oxide species presents in the electrocatalyst (Fig. 4), also this is in accord with the results of XRD and TEM described above. These results are also supported by the electrochemical behavior in the Pd oxidation/reduction region.

Figure 5 shows the cyclic voltammograms (CV) of the Pd/C, Zn/C, $Pd_{(90)}Zn_{(10)}/C$, $Pd_{(70)}Zn_{(30)}/C$ and $Pd_{(50)}Zn_{(50)}/C$ electrocatalysts after adsorption of methane at 0.05 V while bubbling methane for 1,800 seconds in 0.5 mol L^{-1} H_2SO_4. For all electrocatalysts were observed that the hydrogen adsorption-desorption region (0.05 to 0.5 V vs RHE) is increased partially after adsorption of methane. This indicates the hydrogen desorption in the electrode surface. In the anodic scan was also observed an increase in current, which presumably corresponds to the electrooxidation of the adsorbed species. This effect was more pronounced for $Pd_{(90)}Zn_{(10)}/C$ and $Pd_{(70)}Zn_{(30)}/C$ in comparison with Pd/C and $Pd_{(50)}Zn_{(50)}/C$. The presence of the 10-30% by mass of Zn in the Pd/C electrocatalyst could favor the electrooxidation of methane for other products of higher commercial values, however, further information could be obtained with ATR-FTIR measurements [4].
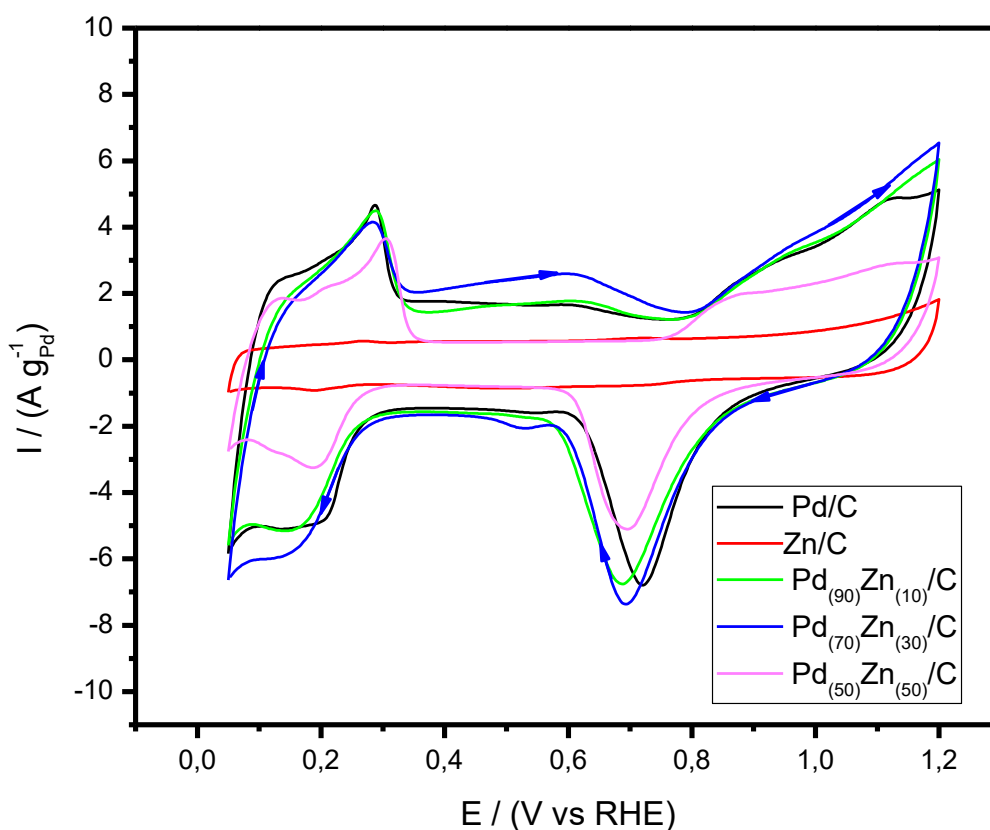
Figure 4. Cyclic voltammograms of Pd/C, Zn/C, $Pd_{(90)}Zn_{(10)}/C$, $Pd_{(70)}Zn_{(30)}/C$ and $Pd_{(50)}Zn_{(50)}/C$ electrocatalysts in 0.5 mol L^{-1} H_2SO_4 solution with a sweep rate of 10 mV s^{-1}.

For Pd/C, $Pd_{(90)}Zn_{(10)}$/C and $Pd_{(70)}Zn_{(30)}$/C electrocatalysts were observed a formation of PdOH (Pd_2O) at 0.619 V and then it is further oxidized to PdO at 0.882 V vs RHE [4, 14]. The oxidation peak increase was more pronounced for $Pd_{(70)}Zn_{(30)}$/C electrocatalyst, indicating that this composition favors the methane oxidation for other products when compared to Pd/C and other electrocatalysts synthesized [23]. This result also could be attributed to higher electron transfer rate for methane oxidation at the formation of PdO at 1.14 V vs RHE, where the Zn oxide also could promote thermal stability via facilitating the redox properties of active PdO phase [41].

The oxidation peak increase was more pronounced for Pd/C, $Pd_{(90)}Zn_{(10)}$/C and $Pd_{(70)}Zn_{(30)}$/C electrodes and its largest surface area than the $Pd_{(50)}Zn_{(50)}$/C and Zn/C. For $Pd_{(90)}Zn_{(10)}$/C and $Pd_{(70)}Zn_{(30)}$/C electrocatalysts also were observed clear shifts of the peak positions to more positive potentials (0.48 V) in the hydrogen adsorption-desorption region when compared to Pd/C and $Pd_{(50)}Zn_{(50)}$/C (both with 0.39 V vs RHE) cyclic voltammograms after adsorption of methane (see Fig. 5). These results agree partly in the work of Zhang et al. [14]. Therefore, this positive shift is an indication of the electronic modification of Pd atoms by the neighboring Zn atoms [37, 42]. This is in accord with the results of XRD described above. The oxidation peak increases after the adsorption of methane, and the reduction peak current at 0.7 V vs RHE doesn't vary, indicating that the oxidation process is irreversible.
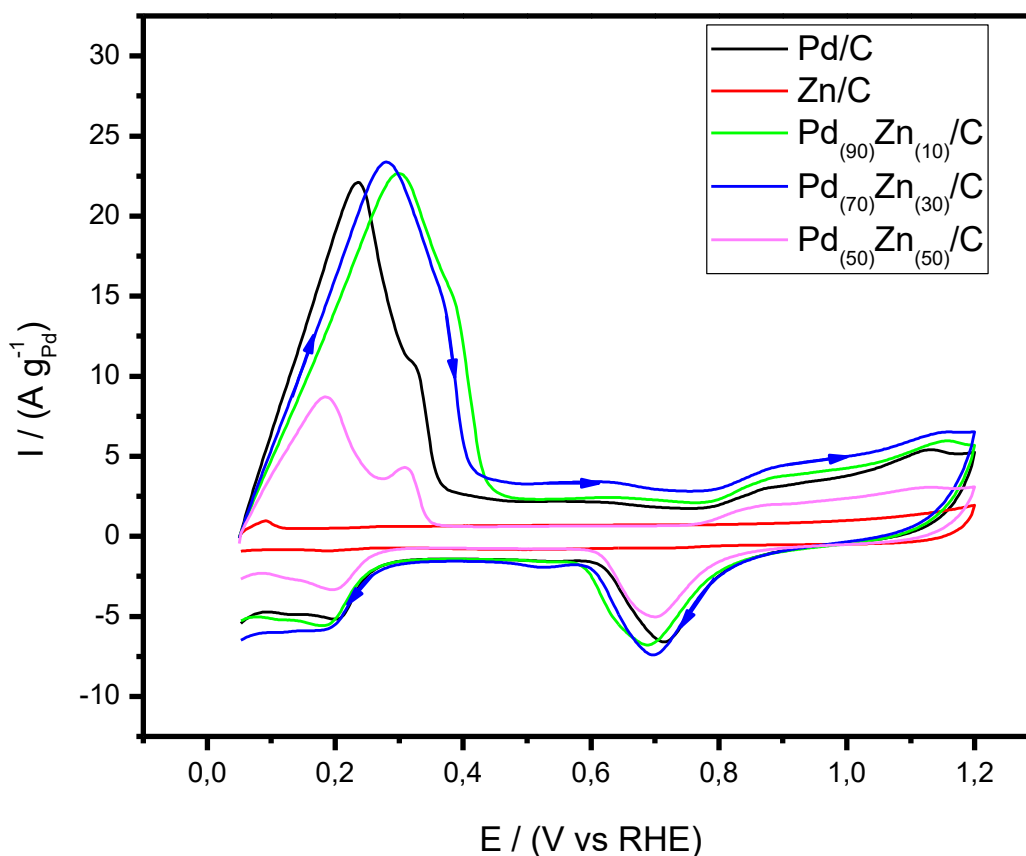

Figure 5. Cyclic voltammograms of Pd/C, Zn/C, $Pd_{(90)}Zn_{(10)}$/C, $Pd_{(70)}Zn_{(30)}$/C and $Pd_{(50)}Zn_{(50)}$/C electrocatalysts, methane (CH_4) passing through the 0.5 mol L^{-1} H_2SO_4 electrolyte for 1,800 seconds.

Figure 6 show the FTIR spectra in the range of 1200 to 850 cm^{-1}, region of mainly products finger print of methane electrochemical oxidation on Pd/C, Pd$_{(90)}$Zn$_{(10)}$/C, Pd$_{(70)}$Zn$_{(30)}$/C, Pd$_{(50)}$Zn$_{(50)}$/C, and Zn/C electrocatalysts). For Pd/C since 0.7 V was possible to see a band close to 1088 cm^{-1} attributed to CH$_3$ rock [43] of methanol and this band increase at 1.2 V, in same potential range the band at 1109 cm^{-1} of the formic acid [44] increase with potential too (Fig. 6a). The band at 1034 cm^{-1} can corresponding both C-O str of methanol [43] and CH bend of formic acid [44].

The Zn addiction on Pd materials cause the appearance of band at $\approx$ 1000 cm^{-1} corresponding to the ν(COH) vibration of methanol and/or ν(COC) in oligomers of the formaldehyde in aqueous solution [45], due to not observed this band in Pd/C, it is possible to linked in this spectra with formaldehyde production from 0.4 V for Pd$_{(90)}$Zn$_{(10)}$ and in all potentials for other PdZn materials (Fig. 6b, 6c and 6d). For Zn/C it is possible to notice a negative band associate with the SO and OH stretching vibrational mode [46] indicating a consumption of the H$_2$SO$_4$ specie, probably due to reaction of SO$_4$ and Zn (Fig. 6e). We results indicated that methane oxidation occurs by parallel mechanisms, with Zn activating a formaldehyde way. Another point is that products formation is not coincident with higher currents in cyclic voltametric experiments.
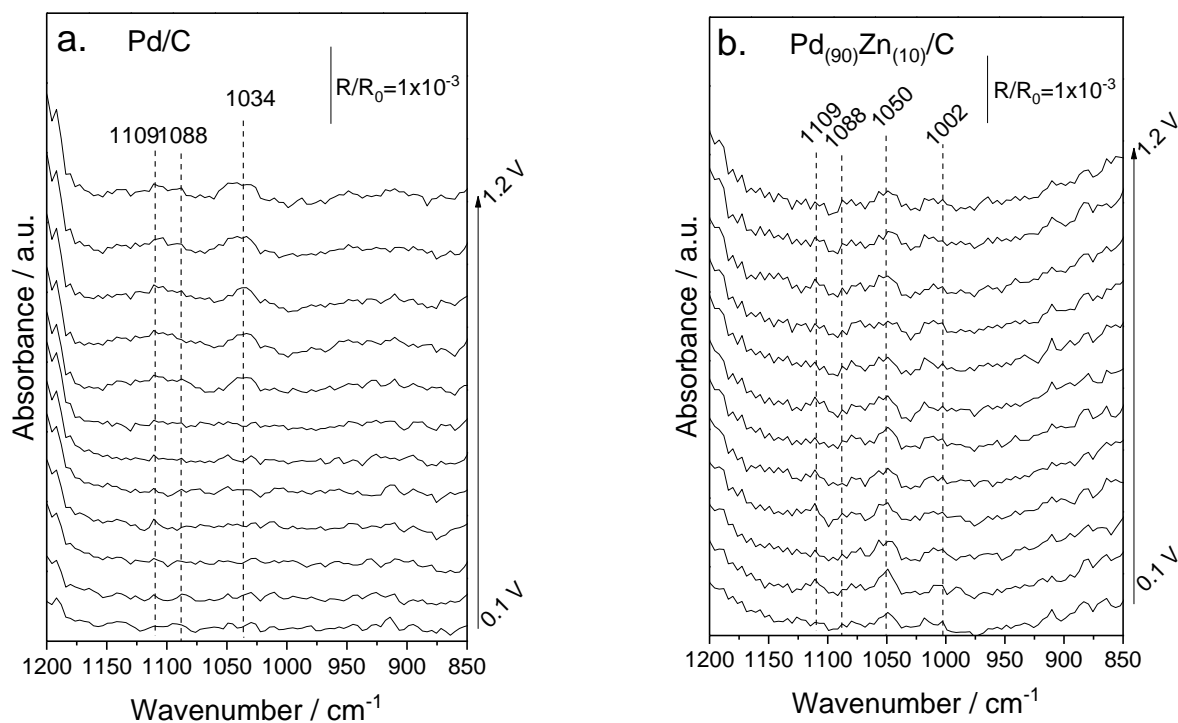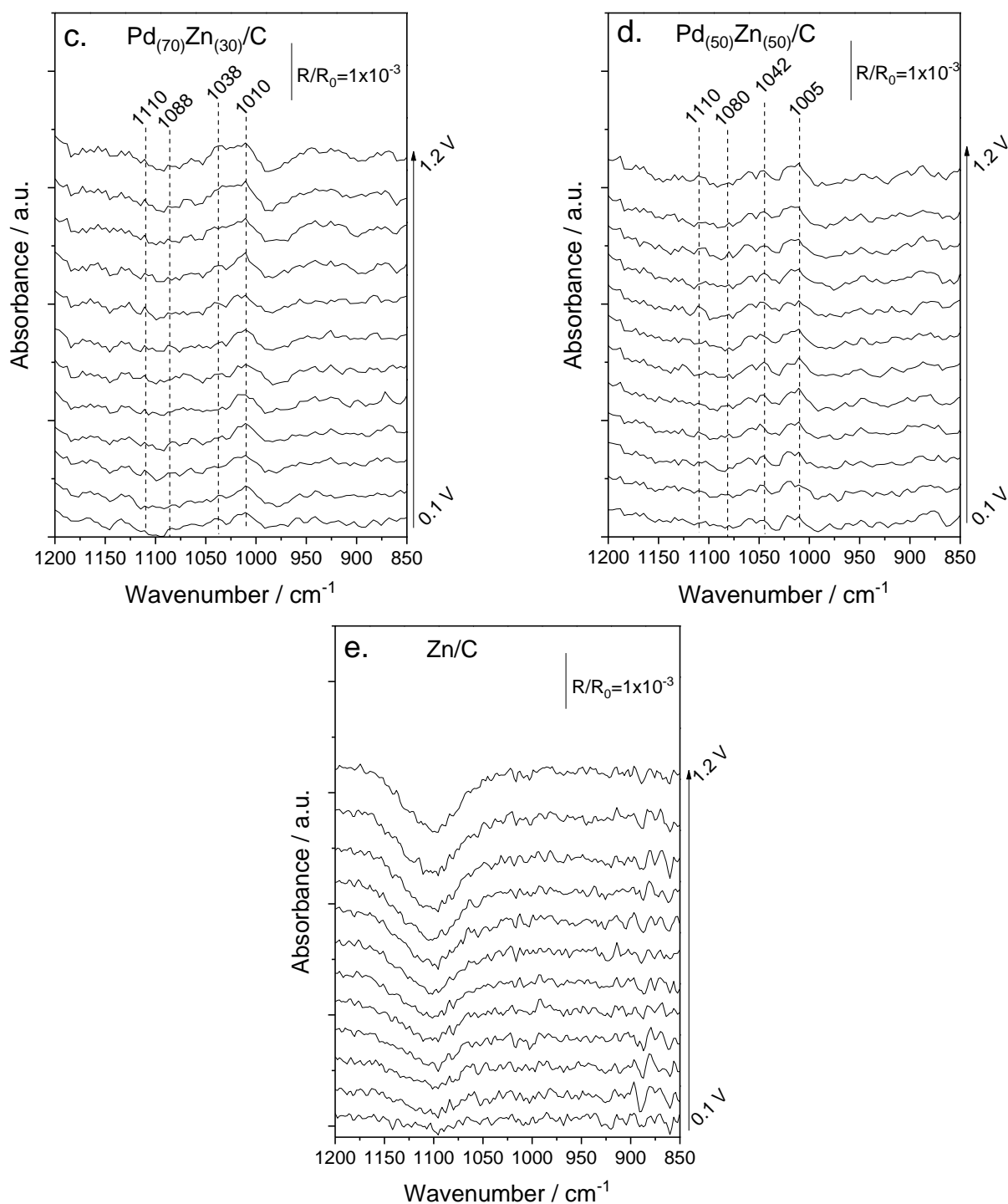
Figure 6. In situ ATR-FTIR spectra in the range of 1200 cm^{-1} to 850 cm^{-1} of methane (CH$_4$) electrooxidation on **(a)**. Pd/C, **(b)**. Pd$_{(90)}$Zn$_{(10)}$/C, **(c)**. Pd$_{(70)}$Zn$_{(30)}$/C, **(d)**. Pd$_{(50)}$Zn$_{(50)}$/C, and **(e)**. Zn/C electrocatalysts at potentials range from 0.05 to 1.2 V with an interval of 0.1 V.

Figure 7 shows the polarization and power density curves obtained in a single proton exchange membrane fuel cells using Pd/C, Zn/C, Pd$_{(90)}$Zn$_{(10)}$/C, Pd$_{(70)}$Zn$_{(30)}$/C and Pd$_{(50)}$Zn$_{(50)}$/C as anode electrodes. Pd/C and Pd$_{(50)}$Zn$_{(50)}$/C electrocatalysts indicate the highest value of maximum power density (0.48 mW cm^{-2} in 3.66 mA cm^{-2} and 0.46 mW cm^{-2} in 3.36 mA cm^{-2}) respectively, while Zn/C

and $Pd_{(70)}Zn_{(30)}$/C (0.32 mW cm^{-2} in 2.31 mA cm^{-2} and 0.38 mW cm^{-2} in 3.16 mA cm^{-2}), respectively. The experiments at 80°C showed that the addition of 10% Zn into Pd/C electrocatalyst promote methane electrooxidation. $Pd_{(90)}Zn_{(10)}$/C showed superior performance for methane oxidation (0.53 mW cm^{-2} in 3.51 mA cm^{-2}), while Zn/C and $Pd_{(70)}Zn_{(30)}$/C indicated a decrease in kinetics reaction.
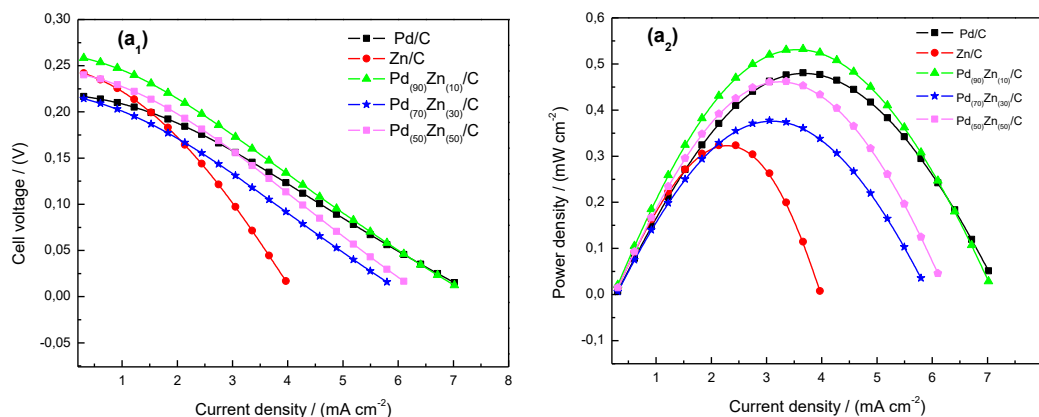
Figure 7. (a_1). Polarization and **(a_2).** power density curves of a 5 cm^2 direct methane fuel cell using 20 wt.% PdZn materials in anode and Pt/C at the cathode (1 mg Pt cm^{-2}) and Nafion® 117 as a membrane at 80°C using 150 mL min^{-1} of methane (CH_4).

4. CONCLUSIONS

Binaries PdZn/C prepared by sodium borohydride reduction method were an efficient electroctrocatalysts for methane activation. For PdZn/C electrocatalysts were observed four peaks at about $2\theta \approx 40°$, 47°, 67° and 82°, which are associated with the (111), (200), (220) and (311) crystal planes, respectively, characteristic of the face-centered cubic structure (fcc) of palladium (Pd); however, a presence of Zn is not observed. For XPS results, Zn/C and $Pd_{(50)}Zn_{(50)}$/C showed the presence of ZnO, but $Pd_{(90)}Zn_{(10)}$/C and $Pd_{(70)}Zn_{(30)}$/C don't mainly because of the lower atomic concentration. Also, all electrocatalysts, except Pd/C, have the presence of Zn^0.

In the scan anodic of PdZn/C electrocatalysts were observed an increase in current in the hydrogen desorption region, however does not correspond to product formation potentials indicating that methane oxidation occurs by parallel mechanisms, as a observed by ATR-FTIR *in situ*.

The experiments at 80°C in PEMFC showed that the addition of 10% Zn into Pd/C electrocatalyst promote methane activation. $Pd_{(90)}Zn_{(10)}$/C showed superior performance for methane oxidation, while Zn/C and $Pd_{(70)}Zn_{(30)}$/C indicated a decrease in kinetics reaction.

Further research is necessary to investigate the mechanisms of methane activation in alkaline electrolytes using PdZn/C electrocatalysts.

References

1. M. Joglekar, V. Nguyen, S. Pylypenko, C. Ngo, Q. Li, M. E. O'Reilly, T. S. Gray, W. A. Hubbard, T. B. Gunnoe, A. M. Herring and B. G. Trewyn, *J. Am. Chem. Soc.,* 138 (2016) 116.
2. R. A. Kerr, *Science*, 328 (2010) 1624.
3. S. Tyagia, A. Ganesh and P. Aghalayam, *ECS Transactions*, 6 (2008) 371.
4. J. Nandenha, E. H. Fontes, R. M. Piasentin, F.C. Fonseca and A. O. Neto, *J Fuel Chem Technol*, 46 (2018) 1137.
5. S. Xie, S. Lin, Q. Zhang, Z. Tian and Y. Wang, *J. Energ. Chem.*, 27 (2018) 1629.
6. N. J. Gunsalus, A. Koppaka, S. H. Park, S. M. Bischof, B. G. Hashiguchi, and R. A. Periana, *Chem. Rev.,* 117 (2017) 8521.
7. M. Joglekar, S. Pylypenko, M. M. Otting, J. S. Valenstein and B. G. Trewyn, *Chem. Mater.,* 26 (2014) 2873.
8. M. Lersch and M. Tilset, *Chem. Rev.,* 105 (2005) 2471.
9. J. A. Labinger, *J. Mol. Catal. A: Chem.,* 220 (2004) 27.
10. A. M. C. Wittborn, M. Costas, M. R. A. Blomberg and P. E. M. Siegbahn, *J. Chem. Phys.*, 107 (1997) 4318.
11. P. E. M. Siegbahn, *J. Am. Chem. Soc.,* 118 (1996) 1487.
12. D. Schröder, H. Schwarz, Angew. *Angew. Chem., Int. Ed. Engl.*, 34 (1995) 1973.
13. Y.-H. (C). Chin, C. Buda, M. Neurock and E. Iglesia, *J. Am. Chem. Soc.,* 135 (2013) 15425.
14. Y. Zhang, L. Zhang, S. Shuang, F. Feng, J. Qiao, Y. Guo, M. M. F. Choi and C. Dong, *Anal. Lett.*, 43 (2010) 1055.
15. G. Psofogiannakis, A. St-Amant and M. Ternan, *J. Phys. Chem. B*, 110 (2006) 24593.
16. M. A. Matin, A. Kumar, R. R. Bhosale, M. A. H. Saleh Saad, F. A. Almomani and M. J. Al-Marri, *RSC Adv.*, 7 (2017) 42709.
17. K. Eid, Y. H. Ahmad, S. Y. AlQaradawi and N. K. Allam, *Catal. Sci. Technol.*, 7 (2017) 2819.
18. M. A. Matin, E. Lee, H. Kim, W.-S. Yoon, and Y.-U. Kwon, *J. Mater. Chem. A*, 3 (2015) 17154.
19. Z. J. Mellinger, T. G. Kelly and J. G. Chen, *ACS Catal.*, 2 (2012) 751.
20. C.-T. Hsieh, P.-Y. Yu, D.-Y. Tzou, J.-P. Hsu and Y.-R. Chiu, *J. Electroanal. Chem.*, 761 (2016) 28.
21. Y. Ren, S. Zhang and H. Li, *Int. J. Hydrogen Energy,* 39 (2014) 288.
22. Y. Song, X. Zhang, S. Yang, X. Wei and Z. Sun, *Fuel*, 181 (2016) 269.
23. F. Hahn and C. A. Melendres, *Electrochim. Acta*, 46 (2001) 3525.
24. P. Jacquinot, B. Müller, B. Wehrli and P. C. Hauser, *Anal. Chim. Acta*, 432 (2001) 1.
25. K. W. Frese, *Langmuir*, 7 (1991) 13.
26. M. Jafarian, M. G. Mahjani, H. Heli, F. Gobal and M. Heydarpoor, *Electrochem. Commun.*, 5 (2003) 184.
27. X. Zhang, H. Fan, J. Zheng, S. Duan, Y. Huang, Y. Cui and R. Wang, *Catal. Sci. Technol.,* 8 (2018) 4757.
28. Z. Li, J. Gao, X. Xing, S. Wu, S. Shuang, C. Dong, M. C. Paau and M. M. F. Choi, *J. Phys. Chem. C*, 114 (2010) 723.
29. A. O. Neto, M. Brandalise, R. R. Dias, J. M. S. Ayoub, A. C. Silva, J. C. Penteado, M. Linardi, E. V. Spinacé, *Int. J. Hydrogen Energy,* 35 (2010) 9177.
30. S. G. Da Silva, E. H. Fontes, M. H. M. T. Assumpção, M. Linardi, E. V. Spinacé, J. C. M. Silva and A. O. Neto, *Ionics,* 23 (2017) 2367.
31. M. C. L. Santos, J. Nandenha, J. M. S. Ayoub, M. H. M. T. Assumpção and A. O. Neto, *J Fuel Chem Technol*, 46 (2018) 1462.
32. C. V. Pereira, E. H. Fontes, J. Nandenha, M. H. M. T. Assumpção and A. O. Neto, *Int. J. Electrochem. Sci.*, 13 (2018) 10587.

33. M. H. M. T. Assumpção, J. Nandenha, G. S. Buzzo, J. C. M. Silva, E. V. Spinacé, A. O. Neto and R. F. B. De Souza, *J. Power Sources*, 253 (2014) 392.
34. J. Guo, R. Chen, F.-C. Zhu, S.-G. Sun and H. M. Villullas, *Appl. Catal., B: Environ.*, 224 (2018) 602.
35. C. Xia, Z. Qiao, C. Feng, J.-S. Kim, B. Wang and B. Zhu, *Materials*, 11 (2018) 40.
36. T. Conant, A. M. Karim, V. Lebarbier, Y. Wang, F. Girgsdies, R. Schlögl and A. Datye, *J. Catal.*, 257 (2008) 64.
37. J. Nandenha, R. F. B. De Souza, M. H. M. T. Assumpção, E. V. Spinacé and A. O. Neto, *Ionics*, 19 (2013) 1207.
38. E. H. Fontes, C. E. D. Ramos, J. Nandenha, R. M. Piasentin, A. O. Neto and R. Landers, *Int. J. Hydrogen Energy,* 44 (2019) 937.
39. H. W. Xiao-Zi Yuan and J. Zhang, *Springer-Verlag London Springer,* 2008.
40. B. S. Solanki and C. V. Rode, *J. Saudi Chem. Soc.*, (2018) *doi:* https://doi.org/10.1016/j.jscs.2018.08.009.
41. J. J. Willis, E. D. Goodman, L. Wu, A. R. Riscoe, P. Martins, C. J. Tassone and M. Cargnello, *J. Am. Chem. Soc.,* 139 (2017) 11989.
42. M. D. Obradović, J. R. Rogan, B. M. Babić, A. V. Tripković, A. R. S. Gautam, V. R. Radmilović and S. Lj. Gojković, *J. Power Sources*, 197 (2012) 72.
43. K. Hamada and H. Morishita, *Sci. Bull. Fac. Educ. Nagasaki Univ.*, 26 (1975) 39.
44. B. S. Beckingham, N. A. Lynd and D. J. Miller, *J. Membr. Sci.*, 550 (2018) 348.
45. K. Z. Gaca-Zając, B. R. Smith, A. Nordon, A. J. Fletcher, K. Johnston, J. Sefcik, *Vib. Spectrosc*, 97 (2018) 44.
46. M. Yamaguchi and A. Ohira, *Comput. Theor. Chem*., 1089 (2016) 54.